Semi-annual Technical Report
for the Period 7/1/71 - 12/31/71

Conduction Mechanisms in Thick
Film Microcircuits

Grant Number: DAHC15-70-G7

ARPA Order No.: 1642

Grantee: Purdue Research Foundation

Principal Investigator: R.W. Vest
(317) 494-4445

Effective Date of Grant: 7/1/70

Grant Expiration Date: 6/30/73

Amount of Grant: $112,458

February 1, 1972

50

Forward

The research described in this report constitutes the third six months effort under a grant from the Advanced Research Projects Agency, Department of Defense under the technical cognizance of Dr. Norman Tallan, Aerospace Research Laboratories, United States Air Force. The research was conducted in the Turner Laboratory for Electroceramics, School of Electrical Engineering and School of Materials Science and Metallurgical Engineering, Purdue University, Lafayette, Indiana 47907, under the direction of Professor R.W. Vest. Contributing to the project were Visiting Assistant Professor G.L. Fuller, Mr. D.J. Deputy, Mr. K.N. Sheely, Jr., and Mr. J.L. Wright.

Table of Contents

List of Figures

I. Introduction

The current status of thick film technology as applied to conductive and resistive formulations is largely the result of empirical developments. The development of new materials as well as the improvement of existing systems have been hindered by an inadequate understanding of the mechanisms by which electric charge is transported in thick film resistors and conductors.

One of the factors that any model for conduction in thick film microcircuits must explain is the fact that the temperature coefficient of resistance (TCR) of a resistor is much lower than the TCR of any of the individual ingredients from which it was made. Several possible approaches to explaining this "TCR anomaly" which are being explored in this project are:

1. Changes in contact resistance between adjacent particles due to thermal stresses,
2. Changes in the intrinsic properties of the conductive material during processing,
3. Formation of new phases which contribute to the conduction,
4. Size effects which change the intrinsic properties of the conductive,
5. Changes in the geometry factor with temperature.

Published work concerning these possible mechanisms was discussed in the first report on this project [1].

The primary thrust of the experimental program is to relate the electrical properties of the thick films to the material properties and processing conditions through microstructure. The materials proper-

ties to be correlated are: resistivity; temperature coefficient of resistivity; coefficient of thermal expansion; interfacial energy; particle shape, size, and size distribution; and chemical reactivity with other constituents. The processing conditions to be correlated are time, temperature, and atmosphere during firing.

The specific objectives of the program are:

1. Determine the dominant sintering mechanisms responsible for microstructure development, and establish the relative importance of the various properties of the ingredient materials.
2. Determine the dominant mechanisms limiting electrical charge transport, and establish the relative importance of the various properties of the ingredient materials.
3. Develop phenomological models to inter-relate the various material properties with system performance.

A proposed model to satisfy objective 1 above is presented in this report, and an experimental program is being developed to test the various aspects of the model. Comments on the proposed model are solicited from the readers of this report to help guide future development.

A major problem in reaching an understanding of typical industrially processed thick film resistor and conductor systems is the complexity of the total manufacturing operation. The large number of variables which influence the value of the resistor make it extremely difficult to purposely change one variable and be certain that some other variable is not changing unexpectedly and completely distorting the meaning of the experimental data. In particular, many resistor systems have small amounts of ingredients added because experience has shown that they improve TCR, stability, etc. From the standpoint of scientific understanding, however, they only cause confusion.

It is felt that the only way to reach an understanding of thick film resistors and conductors is to first perform experiments with the basic ingredient materials and to limit the variety of experimental samples to those that are as conceptually simple and easy to define as possible. This was the procedure followed in the initial phase of this project in an attempt to identify the important material properties and processing variables, and to determine their influence individually on system performance.

The effort during the current reporting period has continued some of the single component experiments, but studies have also been initiated to achieve control of variables in the complete thick film manufacturing process. A precision screen printer has been obtained and put into operation, and screen fabrication techniques have been standardized. A cone and plate viscometer has been obtained and calibrated with standard fluids. A laboratory scale tunnel kiln has been installed and initial check-out completed. It is not the purpose of this project to study screen printing, ink rheology, or tunnel kiln profiling, but these areas must be considered to an extent sufficient to establish their contribution to observed variations in processed films. Some of our initial efforts along these lines are discussed in this report.

II. Theoretical Considerations

A. Microstructure Model

1. Development of Model

Thick film resistors are composite systems consisting of two or more phases. The electrically conducting phase (or phases) is present in the formulation as discrete particles (or as a homogeneous solution

in the case of resinate systems), but must develop into a physically continuous network along the length of the resistor during the firing operation. One of the primary goals of this project is to relate the final microstructure and the kinetics of its formation to the physical properties of the ingredient materials. This section presents a model that is consistent with both current theories of ceramic microstructure development (sintering, etc), and several observations commonly reported for thick-film resistor systems. In particular, for a resistor formulation consisting of discrete particles of a glass and a crystalline, electrically conducting phase, the following observations are predicted:

a. The conducting phase must include an oxide or an oxidizable metal for the resistance to vary continuously over a wide composition range (volume fraction of glass to conductive).
b. Resistor properties are different for different glasses with the same conductive.
c. The changes in resistor properties for different conductives and the same glass are not simply related to the different electrical properties of the conductives.
d. Resistor properties vary with the particle size distribution of the conductive.
e. Extended firing results in an "open" resistor.
f. Good resistors can be made with volume fractions of conductive far less than that required for a continuous conductive phase assuming random distribution.
g. The TCR of the resistor is much less than the TCR of the conductive.

Figure 1 depicts the basic steps in the proposed formation of the microstructure. Thick-film resistor inks consist basically of mixtures

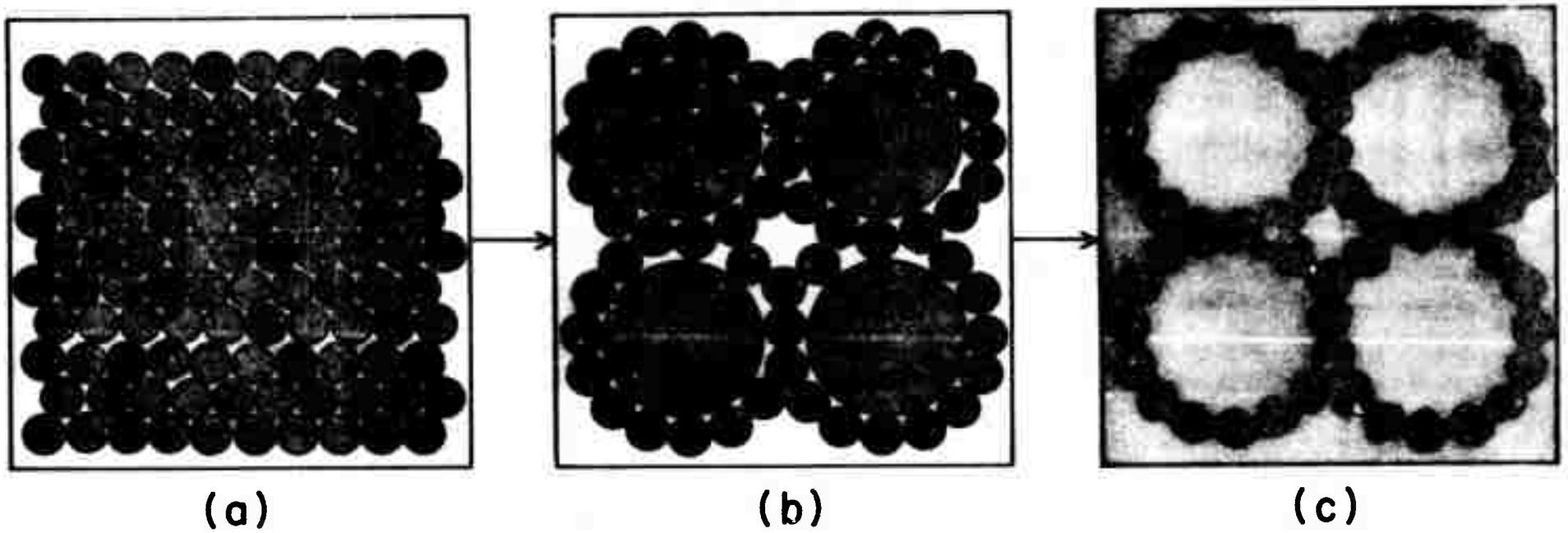

Figure 1. Proposed Model for Resistor Microstructure Development

of glass powder, conductive powder and a screening agent that is removed during drying and the early stages of firing. Figure 1 (a) shows the structure of the film at this stage; the dark areas represent the conductive particles dispersed among the glass particles that are grey in the figure. As the temperature continues to rise, the relative interfacial energies of the glass and the conductive cause the glass particles to sinter and flow together to form larger particles and neighboring conductive particles are pulled together by a thin layer of glass that forms on their surfaces. This structure is represented in Figure 1 (b). While in this configuration the conductive particles begin to sinter together to form the continuous network that is required for a non-insulating structure. As the firing procedure continues, the conductive sintering moves toward completion, and the glass flows to fill the remaining voids, encapsulating the network as shown in Figure 1 (c). For resistor fabrication the process should be terminated at stage (c), but the same driving forces responsible for arriving at this stage lead to a ripening process during which the smaller conductive particles dissolve and reprecepitate on larger conductive particles. The physically continuous conductive network is eventually destroyed by this ripening process.

In the next several parts of this section, the proposed sequence of events are discussed in greater detail, equations are developed that describe the significant reactions and the predictions of resistor properties based on microstructure considerations are demonstrated. The important material properties that emerge are: (1) surface tension, viscosity, and particle size of the glass; (2) sur-

face energy, self diffusion coefficient, particle size, and particle size distribution of the conductive; and (3) the intercomponent effects of interfacial energy, solubility of the conductive in the glass, and diffusion coefficient of the conductive in the glass. The electrical conductivity of the conductive is not a critical property as long as it is sufficiently high so as not to limit the charge transport. The model can be tested by direct optical or SEM techniques that imploy a hot stage and/or by comparison to the predictions of the appropriate equations. If the microstructure model stands the test of experiment it can be used to predict optimum combinations of the pertinent material properties and processing conditions.

2. Glass Sintering

Although several reviews of sintering exist [2-5] the equations important for the microstructure model will be developed for completeness and so that the assumptions made will become apparent.

Consider a system containing two phases with pressures and volumes P_1, V_1, and P_2, V_2. The Gibbs' free energy for this system at constant temperature is

$$G = -V_1P_1 - V_2P_2 + \gamma A. \tag{1}$$

where γ is the interfacial energy of the interface of area A separating the two phases. For a single component system at constant total volume ($V = V_1 + V_2$) in equilibrium

$$dG = 0 = -P_1dV_1 - P_2dV_2 + \gamma dA \tag{2}$$

and since $dV_1 = -dV_2$,

$$P_1 - P_2 = \gamma \frac{dA}{dV_1}. \tag{3}$$

It can be shown that

$$\frac{dA}{dV} = \frac{1}{r_1} + \frac{1}{r_2} \tag{4}$$

where r_1 and r_2 are the principal radii of curvature of the interface at a point (the radii observed in orthogonal planes). The radii are positive for a convex and negative for a concave condensed phase. Combining Eqs. 3 and 4 gives

$$P_1 - P_2 = \gamma \left(\frac{1}{r_1} + \frac{1}{r_2}\right). \tag{5}$$

For a planar interface $r_1 = r_2 = \infty$, and $P_1 = P_2 = P_o$. If we define $\Delta P_1 \equiv P_1 - P_o$ and $\Delta P_2 - P_o$, Eq. 5 becomes

$$\Delta P_1 - \Delta P_2 = \gamma \left(\frac{1}{r_1} + \frac{1}{r_2}\right). \tag{6}$$

Since the phases are in equilibrium and $\Delta G = V\Delta P$ for each phase, $V_1 \Delta P_1 = V_2 \Delta P_2$. If we further assume that phase 2 is the vapor phase and is an ideal gas, then $V_2 \gg V_1$, and Eq. 6 can be written as

$$\Delta P_1 = \gamma \left(\frac{1}{r_1} + \frac{1}{r_2}\right) \tag{7}$$

or

$$\Delta P_2 = \frac{V_1 \gamma}{RT} \left(\frac{1}{r_1} + \frac{1}{r_2}\right) \tag{7'}$$

where R is the gas constant.

For the sintering of two spherical glass particles required to go from stage a to stage b of Figure 1 the geometric relations shown in Figure 2 apply for a viscous flow mechanism; ρ and x are the principal radii of curvature of interest. Since the radius of curva-

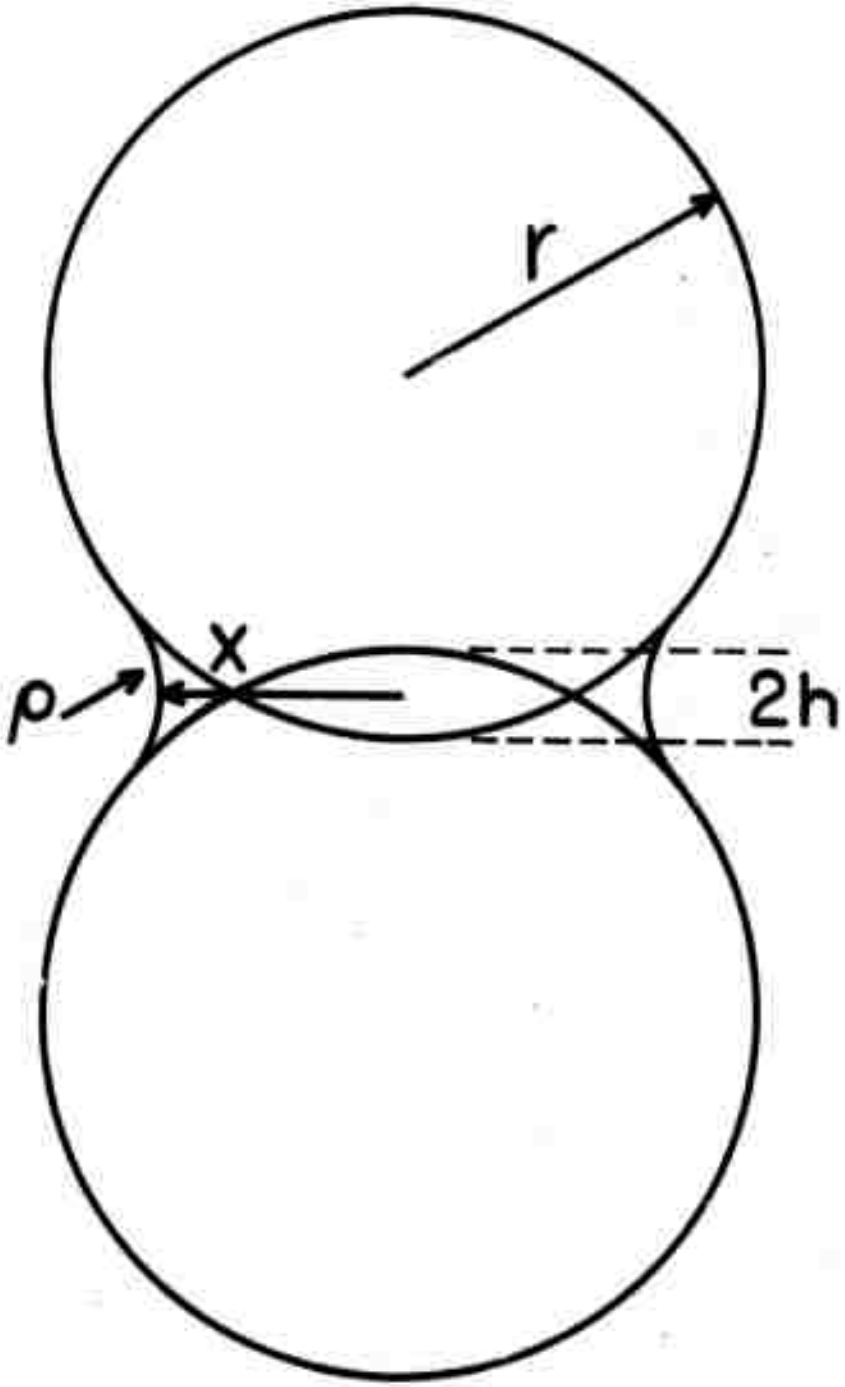

Figure 2. Initial Stage of Viscous Flow Sintering

ture of the neck, ρ, is much less than the radius of the neck, x, Eqs. 7 and 7′ simplify to

$$\Delta P_1 = \frac{-\gamma}{\rho} \tag{8}$$

and

$$\Delta P_1 = \frac{-V_1 \gamma P_o}{RT\rho} \tag{8'}$$

where the minus sign arises from the fact that ρ is a concave radius with respect to the solid phase. Equation 8 describes the negative pressure or tensile stress acting in the neck region and is the driving force for the sintering process. If the material in the neck region behaves as a viscous Newtonian fluid (i.e. the shear stress is proportional to the shear strain rate) the expression for the time dependence of the neck growth first developed by Frenkel [6] is

$$\frac{x^2}{r} = \frac{3}{2} \frac{\gamma}{\eta} t \tag{9}$$

where η is the viscosity. The shrinkage per sphere is h (Figure 2) and $h \simeq \rho$. For $x/r < 0.3$ it can be shown that $\rho \simeq \frac{x^2}{4r}$. Therefore, the relative change in length of a powder compact is

$$\frac{\Delta L}{L} = \frac{h}{r} = \frac{x^2}{4r^2} \tag{10}$$

Combining Eqs. 9 and 10 gives

$$\frac{\Delta L}{L} = \frac{3\gamma}{4r\eta} t \tag{11}$$

Frenkel's solution has been generalized to non-Newtonian liquids by Kuczynski et. al. [7], but experimental observations [7,8] indicate that the neck growth of glass spheres and cylinders follows Eq. 9.

Equations 9 and 11 which describe the initial stages of the viscous flow sintering mechanism should predict the kinetics for going

from stage a to stage b of Figure 1. The significant material properties involved are surface tension, viscosity, and particle size of the glass, and these are expected to change among different glasses. Hence one would predict different kinetics for different glasses and observation b in part 1 of this section would be expected.

Viscous flow should also be the dominant mechanisms in achieving zero porosity to reach stage c of Figure 1 from stage b where the conductive has only a surface coating of glass. During the final stages of densification there exist spherical pores, but the kinetics of this later stage of sintering are not described by Eq. 11. The pressure inside a spherical pore of radius r_p is given by Eq. 7 as

$$\Delta P = \frac{-2\gamma}{r_p} \tag{12}$$

and this is the driving force for final densification. It can be shown [9] that

$$\frac{d\phi}{dt} = \frac{3\gamma}{2r_o\eta}(1-\phi) \tag{13}$$

where ϕ is the ratio of the density at time t to the theoretical density and r_o is the initial particle radius. Integration of Eq. 13 gives

$$\phi = 1 - \exp\left(\frac{-3\gamma t}{2r_o\eta}\right). \tag{14}$$

Thus it is seen that the same material properties, surface tension, viscosity, and particle size of the glass, control the kinetics of the final densification.

3. Conductive Network Development

Any interaction between a solid phase and a liquid phase requires some degree of wetting of the solid by the liquid. Wetting can be described in terms of a contact angle θ or the interfacial energies

γ_{LV}, γ_{SL}, and γ_{SV} between the liquid/vapor, solid/liquid, and solid/vapor phases respectively. The relationship among these is shown in Figure 3 , and can be described by the equation

$$\gamma_{SV} = \gamma_{SL} + \gamma_{LV} \cos\theta. \tag{15}$$

For complete wetting $\theta = 0$, and $\gamma_{SV} = \gamma_{SL} + \gamma_{LV}$. For partial wetting $\theta < 90^{o}$, and $1 > \frac{\gamma_{SV}-\gamma_{SL}}{\gamma_{LV}} > 0$. For the case of complete wetting of a spherical particle by a liquid the geometry shown in Figure 4 applies. The spherical particles are held together by the liquid because the pressure in the liquid in the neck between the particles is less than the ambient pressure by the ammount of the capillary pressure, equal to

$$P = \frac{-\gamma_{LV}}{\rho} \tag{16}$$

This is the driving force for holding the conductive particles together on the sintered glass surface as required for stage b (Figure 1) of the microstructure model. For example, taking a value of ρ=0.05μm as reasonable for a 1μm particle ($r = 0.5\mu m$), and 500 ergs/cm^2 as a typical surface tension value gives 1500 psi for the force holding the particles together.

The force given by Eq. 16 is more than adequate to bring about the arrangement of conductive particles into a continuous network as they are mechanically agitated during the early stages of the glass sintering. As a result, a continuous network of conductive particles is possible even at low volume fractions in agreement with observation f in part 1 of this section. The significant material properties involved are the surface tension of the glass and of the conductive, the interfacial energy between the glass and conductive, and the particle size of the conductive. Since wetting is required, observation a in part 1 of this section is expected; oxides are wet to a much greater degree by oxide

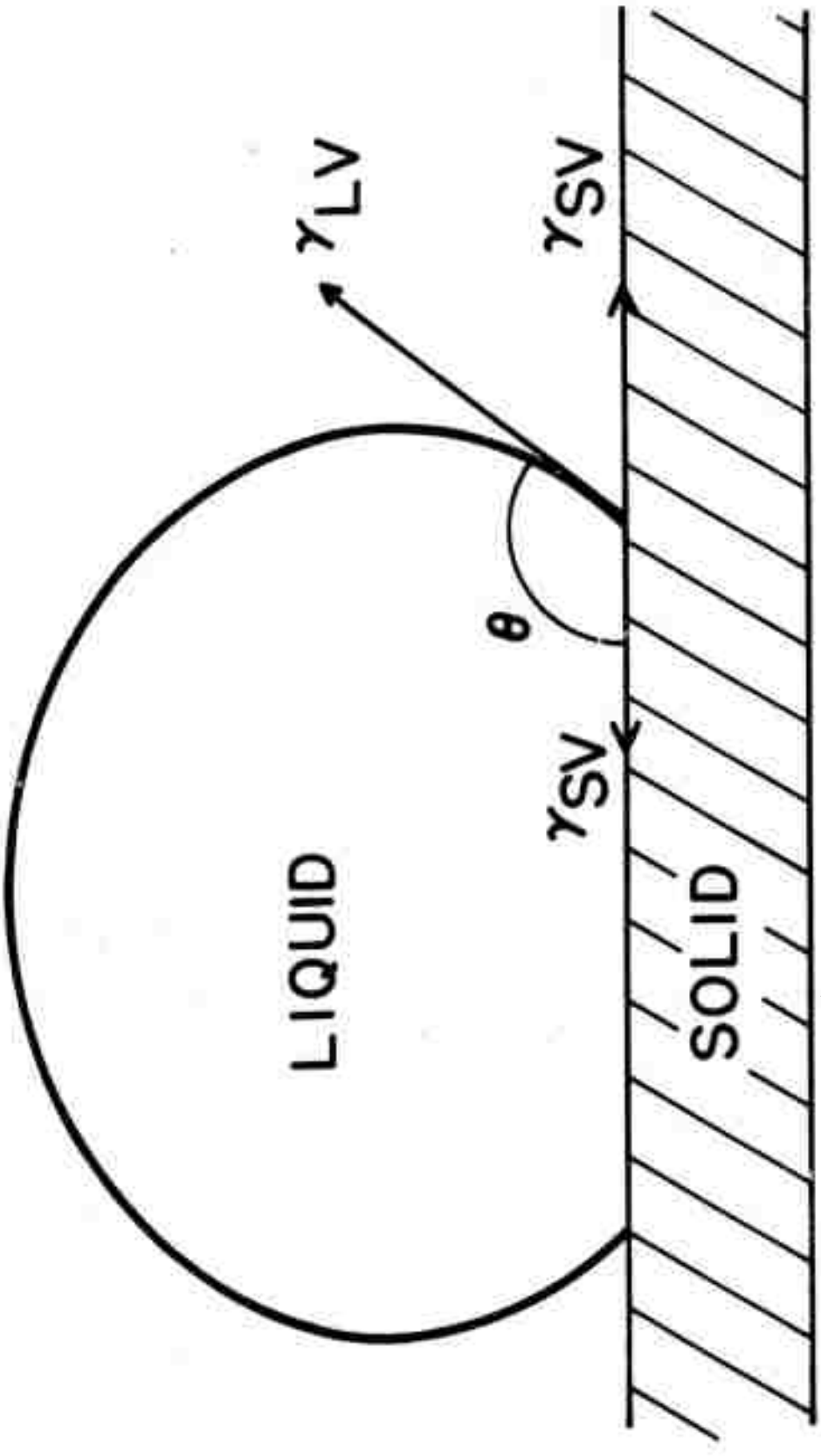

Figure 3. Solid-Liquid-Vapor Interface

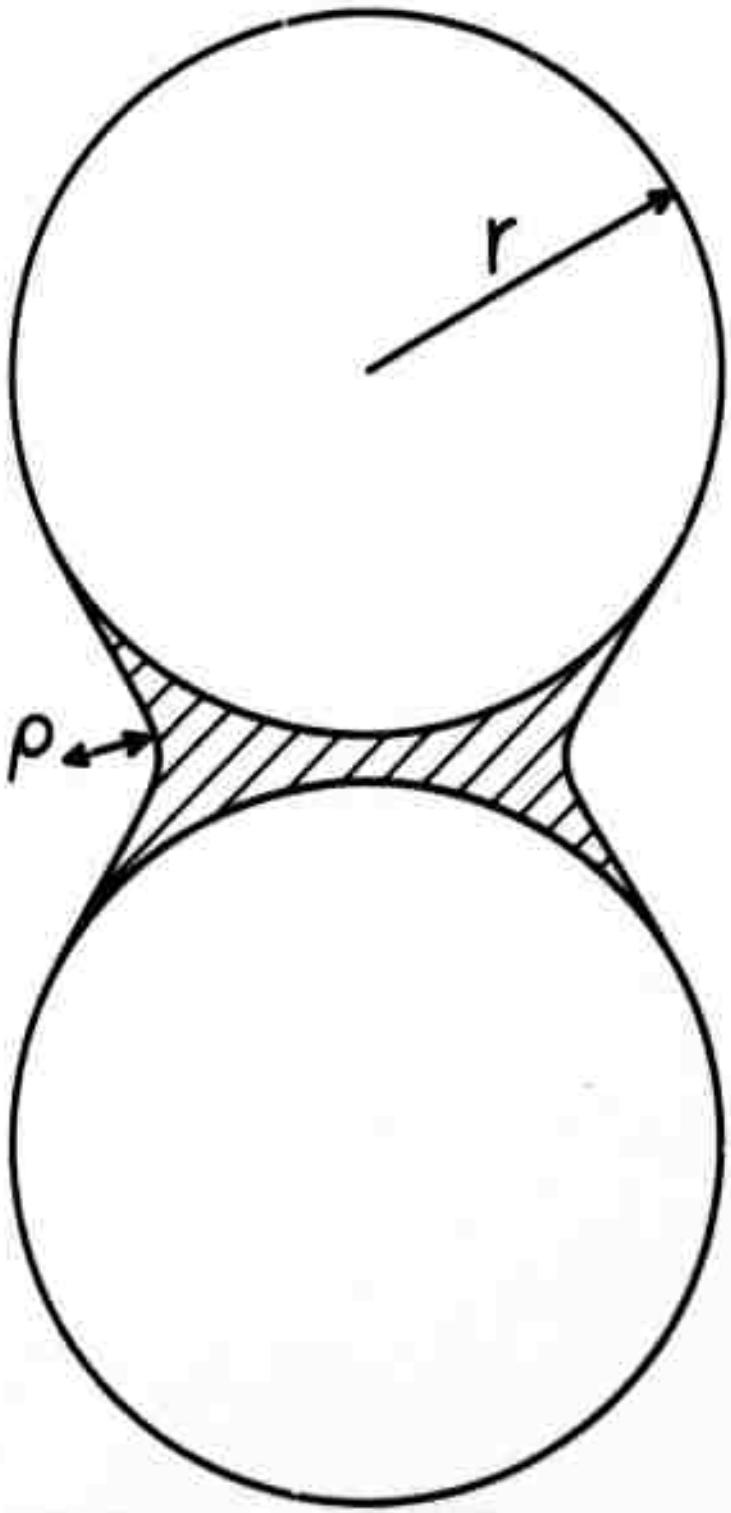

Figure 4. Glass Film Between Conductive Spheres

glasses than are metals. Observations b, c, and d also follow from the significant materials properties for this part of the model.

4. Conductive Sintering

The conductive particles are pulled together by the tensile stress given by Eq. 16. If the glass behaves as a viscous fluid it will be squeezed out of the neck area until the particles are in contact (or with a very thin glass layer spearating them), and the geometry shown in Figure 5 applies. At this point the tensile stress will be counter-balanced by a compressive stress at the conductive/conductive interface. This stress is a driving force for sintering of the conductive particles.

The increase in vapor pressure due to an applied pressure ΔP according to Clapeyron's equation is given by

$$V_c \Delta P = RT \ln \frac{p}{p_o} \tag{17}$$

Combining Eqs. 7 and 17 gives

$$\ln \frac{p}{p_o} = \frac{V_o \gamma}{RT} \left(\frac{1}{r_1} + \frac{1}{r_2}\right) \tag{18}$$

or in more general terms

$$\ln \frac{a}{a_o} = \frac{V_o \gamma}{RT} \left(\frac{1}{r_1} + \frac{1}{r_2}\right) \tag{19}$$

where a is the activity of the conductive and V_o is the molar volume. The driving force represented by Eq. 19 will lead to sintering by either a solid state diffusion or by a solution-dissolution mechanism; these will be discussed separately.

Equation 19 predicts an activity gradient which will result in a flux of matter toward the area under tension and away from the area

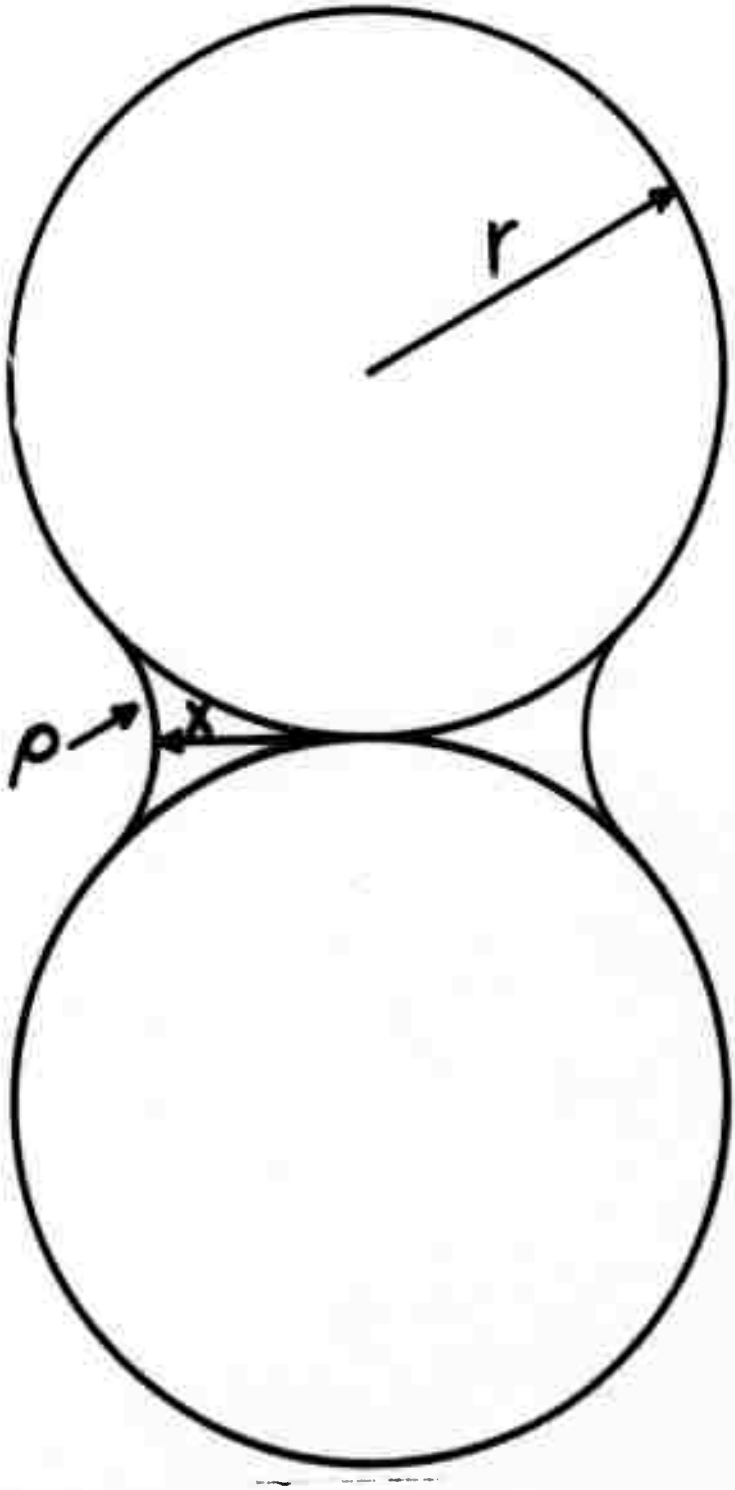

Figure 5. Initial Stage of Bulk Diffusion or Solution-Dissolution Sintering

under compression. This bulk diffusion requires a vacancy sink in the compressional region which can be either an external surface or an internal grain boundary. For the sintering of two solid spheres in the presence of a liquid phase it can be shown [10] that the neck growth for a surface vacancy sink is given by

$$\frac{X^5}{r^2} = \frac{10\gamma_{SL}V_oD}{RT}\,t \tag{20}$$

while for the grain boundary vacancy sink it is given by

$$\frac{X^5}{r^2} = \frac{31\gamma_{SL}V_oD}{RT}\,t \tag{21}$$

where D is the bulk diffusion coefficient. For an oxide, D is the diffusion coefficient of the slower moving species, probably oxygen.

Equation 19 also predicts that the solubility of the conductive in the glass will be changed by the radius of curvature of the interface. For the particles themselves $r_1 = r_2 = r$ and Eq. 19 can be written.

$$\ln\frac{C}{C_o} = \frac{2V_o\gamma_{SL}}{RTr} \tag{22}$$

where C_o is the equilibrium solubility. In the neck region of Figure 5, $r_1 = x$ and $r_2 = -\rho$, but $\rho \ll x$ so Eq. 19 becomes

$$\ln\frac{C}{C_o} = \frac{-V_o\gamma_{SL}}{RT\rho} \tag{23}$$

Equations 22 and 23 predict that there will be an increase in the solubility of the conductive particles and a decrease in the solubility in the neck region causing material from the particles to dissolve and reprecipitate at the neck. The neck growth by this mechanism can be shown [11] to be

$$\frac{X^3}{r} = 6\alpha\gamma_{SL}C_o \left[\frac{V_o^3 d}{2\pi(RT)^3}\right]^{1/2} t \qquad (24)$$

where α is a sticking coefficient and d is the density. It was assumed that the diffusion to the neck region of the conductive dissolved in the glass is fast. If this is not the case the neck growth depends on this diffusion coefficient.

The significant material parameters for the bulk diffusion mechanism are particle size and self diffusion coefficient of the conductive, and the conductive/glass interfacial energy. The significant material parameters for the solution - dissolution mechanisms are the particle size of the conductive, the equilibrium solubility of the conductive in the glass, and the interfacial energy between the conductive and the glass. Particle size distribution is also significant in that smaller particles will dissolve even more rapidly and precipitate in the neck region between larger particles thereby increasing the sintering rate. Observations a, b, c, and d in part 1 of this section follow from these considerations.

Observation g in part 1 of this section is also expected from either of the proposed sintering mechanisms. Some constituents of the glass undoubtedly will remain in the neck area after sintering, and will result in an increased, temperature independent, impurity electron scattering. Even in the absence of impurities, increased temperature independent scattering would be expected due to the imperfect nature of the grain boundary formed. The requirement of small particle size for either sintering mechanism suggests increased surface scattering which is also temperature independent.

5. Ripening

Unfortunately for thick film resistor manufacturers the driving forces for solution - dissolution described by Eqs. 22 and 23 do not disappear when the desired conductive network is formed. The smaller particles will continue to dissolve more rapidly and precipitate on larger particles. This Ostwald ripening process has been treated quantatively [12] to give

$$\bar{r}^3 - \bar{r}_o^3 = \frac{6DC_oM}{d^2RT}\,t \qquad (25)$$

where D is the diffusion coefficient in the liquid, M is the molecular weight, and $\bar{r}$ and $\bar{r}_o$ are the average radii of the particles at times t and zero respectively. Equation 25 assumes isotropic growth, and will not hold strickly for conductives with a preferred growth direction. Continued conductive grain growth as predicted by Eq. 25 will eventually destroy the integrity of the network in accordance with observation e in part 1 of this section.

6. Relative Kinetics

In order to satisfy the microstructure model the glass sintering must occur prior to the conductive sintering. This is the expected order from reported sintering studies, but must be determined for the system of interest. There is no basis at present for choosing either bulk diffusion or solution-dissolution as the dominant conductive sintering mechanism. An experimental study is required to determined which model fits the kinetic data. A choice between the two is important because different material parameters are involved in each.

All of the kinetic equations developed hold only for isothermal sintering, whereas thick film processing involves various heating and cooling rates with short (if any) constant temperature zones. Several

authors [13-16] have considered sintering at constant heating rate. It is first necessary to determine the activation energy (Q) for sintering from a series of isothermal experiments and use of the equation

$$\frac{\Delta L}{L} = K_o \exp\left(\frac{-Q}{RT}\right). \tag{26}$$

Then any of the equations for neck growth or shrinkage can be written in terms of the heating rate y. For example, Eq. 11 for shrinkage by viscous flow becomes [17]

$$\frac{\Delta L}{L} = \frac{4064\gamma R}{y r \eta Q} \exp\left(-\frac{Q + 5800}{RT}\right) \tag{27}$$

After confirming or modifying the sintering model with isothermal experiments it will be necessary to modify the equations for heating rate to approximate thick film processing.

7. Miscellaneous

The way in which several additional factors influence thick film resistors become understandable with the proposed model. The importance of uniform dispersion of the glass and conductive in the formulation is apparent. For a conductive particle to be wet and become part of the network it must be adjacent to a glass particle. Agglomeration of conductive particles would result in fewer of them contributing to the conduction paths.

It should be pointed out that thru-out the model development, it is not simply the magnitudes of the important material properties that are controlling, but rather their relative magnitudes. This is due to the fact that the proposed model requires sequential sintering and particle binding steps, several of which depend on the same material properties but in different ways. The model, therefore, predicts that variations observed in resistor properties with changes in the glass or

conductive are due to a change in the balance among these properties. The same is true for the introduction of additives to formulations. For example, addition of bismuth oxide is known to aid in the formation of certain resistors. The known fluxing action of Bi_2O_3 would reduce the interfacial energy and enhance wetting thereby speed the achievement of stage b of Figure 1. Various other additives may function in a similar manner.

B. Resistor Geometry Effects

Several aspects of thick film processing technology can lead to non-uniform geometries of the fired resistor. When the ink is initially transfered from the screen to the substrate it is present as a series of isolated right cylinders corresponding to the screen mesh. During the leveling process these cylinders merge to form a uniform film. If the leveling process does not proceed to a sufficient extent a waviness with the periodicity of the screen mesh will remain on the resistor surface, while "bleedout" will result if the leveling proceeds too far. "Bleedout" can also occur during firing if the time-temperature product is too high. Improper set-up of the screening machine can lead to varying film thickness along the length or width of the resistor; this thickness variation can be either monotonic or periodic with a period long compared to the screen mesh period.

Thickness variations across the width of a resistor do not cause resistance variations because the cross sectional area along the current path remains constant for a given volume of resistor material deposited. Thickness variations along the length of a resistor do lead to resistance variations for a given volume of resistor material

deposited and these will be considered. For modeling purposes the square wave and saw tooth geometries shown in Figure 6 will be considered. These represent the two limiting cases for thickness variations due to the screen mesh pattern on the resistor surface, and the saw tooth is a good approximation for the monotonic or long period variations. Both geometries are depected in Figure 6 for one cycle but the results will be applicable to any number of cycles because the electrodes at either end are equi-potential surfaces; the waves had to be drawn twice the normal cycle in order to achieve this result.

The resistance of a resistor having the square wave shape shown in Figure 6 (a) and width w can best be determined by conformal mapping techniques. Using suitable coordinate transformations it can be shown [18] that for values of $t_2/t_1 < 1.5$ the number of squares (n) is given by

$$n = \frac{2\ell}{t_1} + \frac{2\ell}{t_2} + \frac{2}{\pi}\left[\frac{(S^2+1)}{S} \ln\left(\frac{S+1}{S}\right) - 2 \ln\left(\frac{4S}{S^2-1}\right)\right] \qquad (28)$$

where $S = t_2/t_1$. The resistance (R) of the film is then

$$R = \frac{n}{w}\rho \qquad (29)$$

where ρ is the resistivity. The resistance of a resistor with the same volume of resistor material but with a flat surface is given by

$$R_o = \frac{4\ell\rho}{wt} = \frac{8\ell\rho}{w(t_1 + t_2)} \qquad (30)$$

where

$$t = (t_1 + t_2)/2.$$

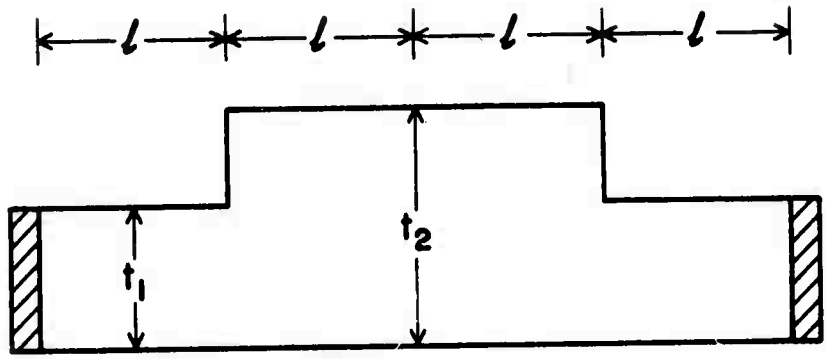

(a) SQUARE WAVE

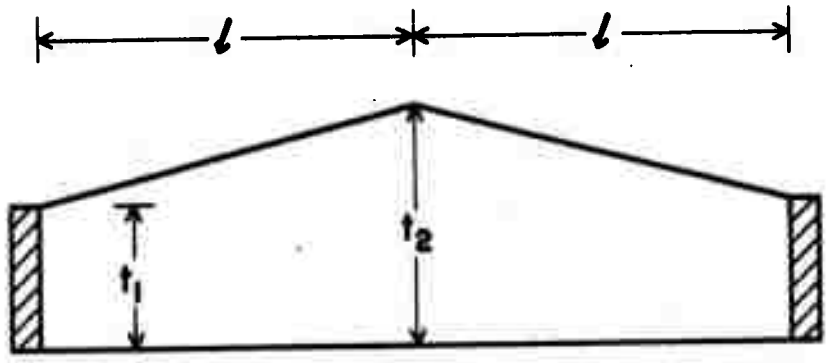

(b) SAW TOOTH

Figure 6. Resistor Geometry Models

Therefore

$$\frac{R}{R_o} = \frac{n(t_1 + t_2)}{8\ell} \tag{31}$$

Substituting the value of n from Eq. 28 and simplifying gives

$$\frac{R}{R_o} = \frac{1}{2} + \frac{S^2 + 1}{S}\left[\frac{1}{4} + \frac{t}{2\pi\ell}\ln\left(\frac{S+1}{S-1}\right)\right] - \frac{t}{\pi\ell}\ln\left(\frac{4S}{S^2-1}\right) \tag{32}$$

Equation 32 can be solved for various values of the parameter t/ℓ. For the problem of the screen pattern surface variation, the value of ℓ can be approximated as the average of the wire diameter and mesh opening. Taking a nominal film thickness (t) of 1 mil (0.001") the dependence of R/R_o on S is plotted in Fig. 7 for four different screen mesh sizes. The deviation of R from R_o is seen to increase rapidly as the amplitude of the surface irregularily increases and reaches 29% at t_2/t_1 equal to 2 for the 325 mesh screen.

The saw tooth geometry of Figure 6 (b) does not lend itself as easily to conformal mapping techniques, but the problem can be solved by using the flux tube approximation. If N_p is the number of flux tubes in parallel along the length of the resistor, and N_s is the number of squares in series in each flux tube then

$$R = \frac{N_s \rho}{N_p \omega} \tag{33}$$

where ρ and ω are the resistivity and width of the resistor as before. N_s can be approximated as the ratio of the average length of a flux tube to the average length of a square to give

$$N_s = \frac{2\ell + 2[\ell^2 + (t_2 - t_1)^2]^{1/2}}{2} \Big/ \frac{\frac{t_2}{N_p} + \frac{t_1}{N_p}}{2} \tag{34}$$

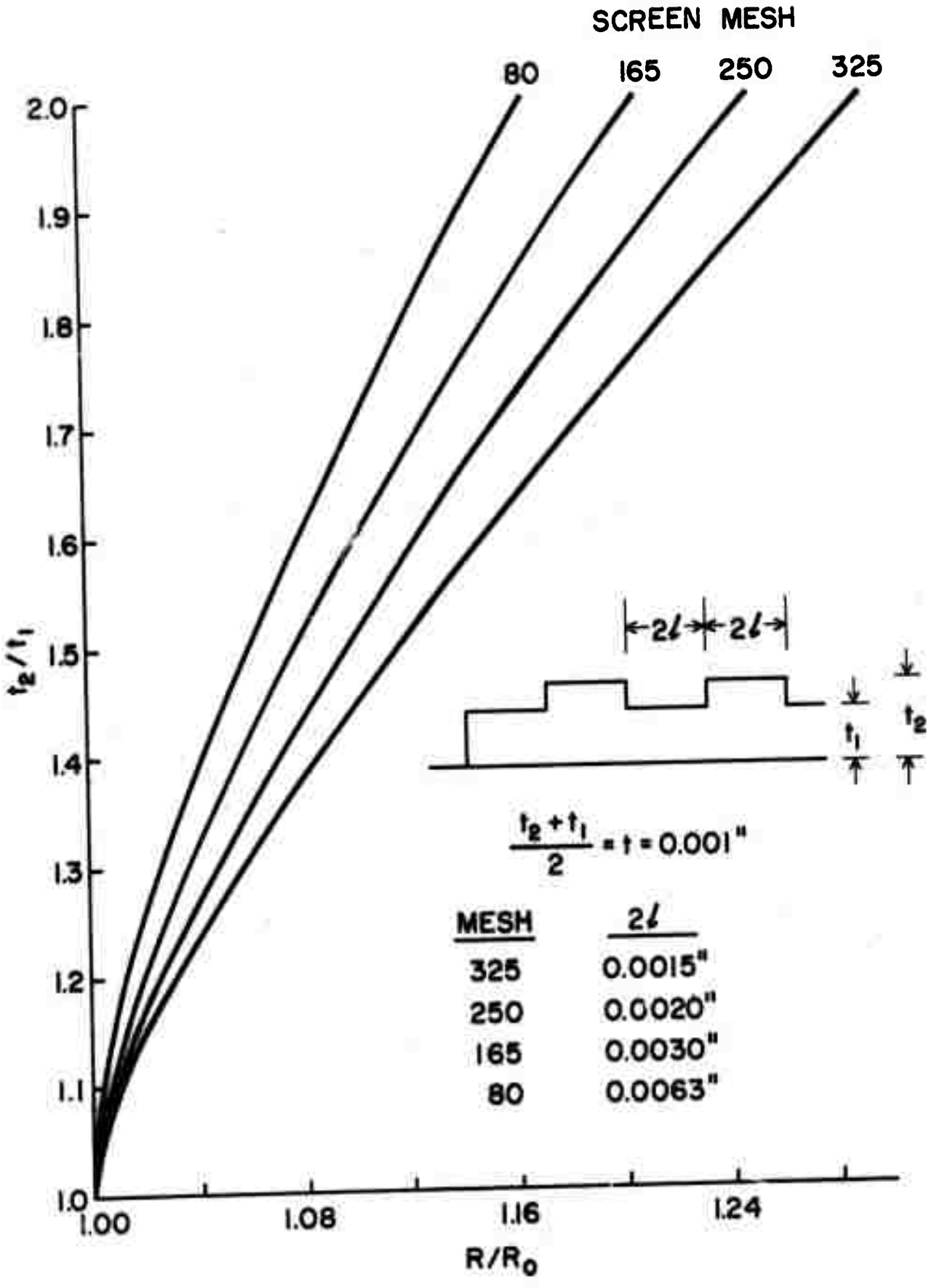

Figure 7. Variation in Resistance with Square Wave Surface Roughness

Combining Eqs. 33 and 34 gives

$$R = \frac{2\ell + 2[\ell^2 + (t_2-t_1)^2]^{1/2}}{t_2 + t_1} \frac{\rho}{\omega} \tag{35}$$

The resistance of a resistor with the same length and width and containing the same volume of resistor material but with a flat surface is given by

$$R_o = \frac{2\ell\rho}{\omega t} \tag{36}$$

where $t = (t_1 + t_2)/2$ as before. Therefore

$$\frac{R}{R_o} = \frac{\ell + [\ell^2 + (t_2-t_1)^2]^{1/2}}{2\ell} \tag{37}$$

Rearranging Eq. 37 to contain the same variables as Eq. 32 gives

$$\frac{R}{R_o} = \frac{1}{2} + \frac{1}{2}\left[1 + 4\left(\frac{t}{\ell}\right)^2 \left(\frac{S-1}{S+1}\right)^2\right]^{1/2} \tag{38}$$

where $S = t_2/t_1$ as before. Calculating ℓ values from the wire diameter and mesh opening, and taking a nominal thickness of 1 mil (0.001") the dependence of R/R_o on S shown in Figure 8 is obtained. A comparison of Figures 7 and 8 shows that the square wave model predicts variations three times as great as the saw tooth. The actual case will lie somewhere between these two extremes, and probably closer to the saw tooth. These figures combined with a measurement of the surface roughness due to the screen pattern can establish limits on the measured resistance variation due to this effect. This may be particularly significant in the present project because no leveling agents will be added to the formulation in order to keep the system as simple as possible.

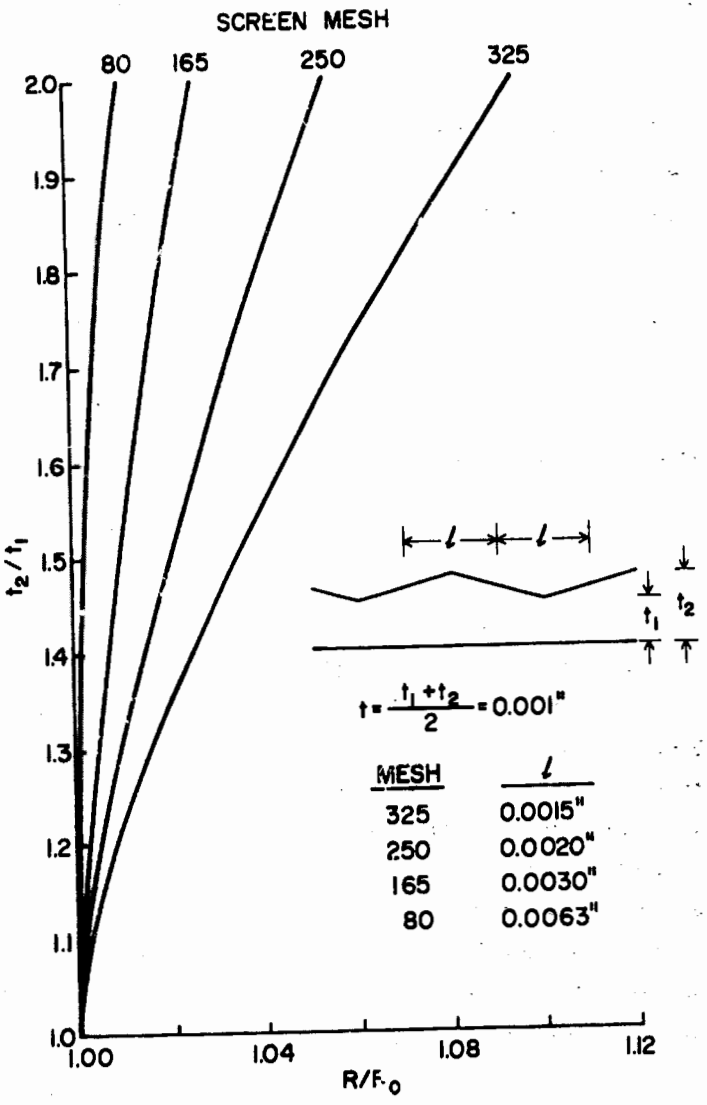

Figure 8. Variation in Resistance with Sawtooth Surface Roughness

Equation 38 can also be used to calculate the deviation in resistance value due to monotonic or long period thickness variations resulting from improper printer set up, but the effect is seen to be small. For example, a 20 mil long resistor 1 mil thick with S = 2 (a more severe case than ever expected in practice) would give $R/R_o = 1.001$, a deviation of only 0.1%.

III. Experimental Studies

A. Contact Resistance of RuO_2

Since one of the proposed models for the conduction mechanism in thick film resistors involves changes in contact resistance between adjacent conductive particles, it is important to determine the change in contact resistance with temperature and pressure in the absence of extraneous factors such as interactions between the conductive and the glass in order to determine the relative contribution of this mechanism. To obtain the necessary data, the resistance of RuO_2 powder compacts was measured as a function of isostatic pressure and temperature in order to extend the room temperature measurements previously reported [1].

The samples were fabricated by isostatically pressing RuO_2 powder (0.5 μm average particle size) in a 5mm diameter cylindrical rubber mold to 55,000 psi in order to develop sufficient green strength. Two 0.13mm diameter, platinum wires were wrapped around the sample along its axis to serve as potential leads, and two platinum plus 10% rhodium wires were wrapped around the sample near its ends to serve as current leads, and also in conjunction with the platinum wires as a temperature measuring thermocouple.

It was necessary to encapsulate the sample in a pliable mold so that isostatic conditions could be realized when immersed in the pressure transmitting fluid. Problems arose in that the General Electric RTV106 used previously [1] as an encapsulant was found to be somewhat permeable to water (the pressure transmitting fluid) at high pressures. After consultation with the supplier it was learned that Silastic 733RTV is completely impervious to hydrocarbons, and this material was then used as a sample encapsulent. A solution of 26.5 w/o diphenyl and 73.5 w/o diphenyl oxide (purchased as Dowtherm A) was found to be more dense than water at all temperatures and pressures of interest. The sample was then placed in a high pressure cell fitted with electrical feed - throughs and filled with Dowtherm A. No mixing of the water and Dowtherm A was observed throughout the experimental program.

The resistivity at room temperature as a function of pressure for one sample is shown in Figure 9. The magnitude of the resistivity in Figure 9 when compared to that of crystalline RuO_2 at room temperature (3.4×10^{-5} Ω - cm) indicates that only contact resistance is being measured. As would be expected for samples of this type the repeatability of the resistivity - pressure data was poor. However, for four different samples, each of which was cycled many times, the resistance change was never as great as a factor of two and usually much less over the pressure range 0-12,000 psi. Therefore, the previous conclusion [1] that "changes in pressure on the contact between adjacent conductive grains due to mismatch among system components is insufficient in itself to compensate for the change in resistance with temperature of the RuO_2 grains", is reaffirmed.

The ratio of the resistivity at zero pressure to the resistivity at 12,000 psi for sample 3E is given in the following table for various elevated temperatures.

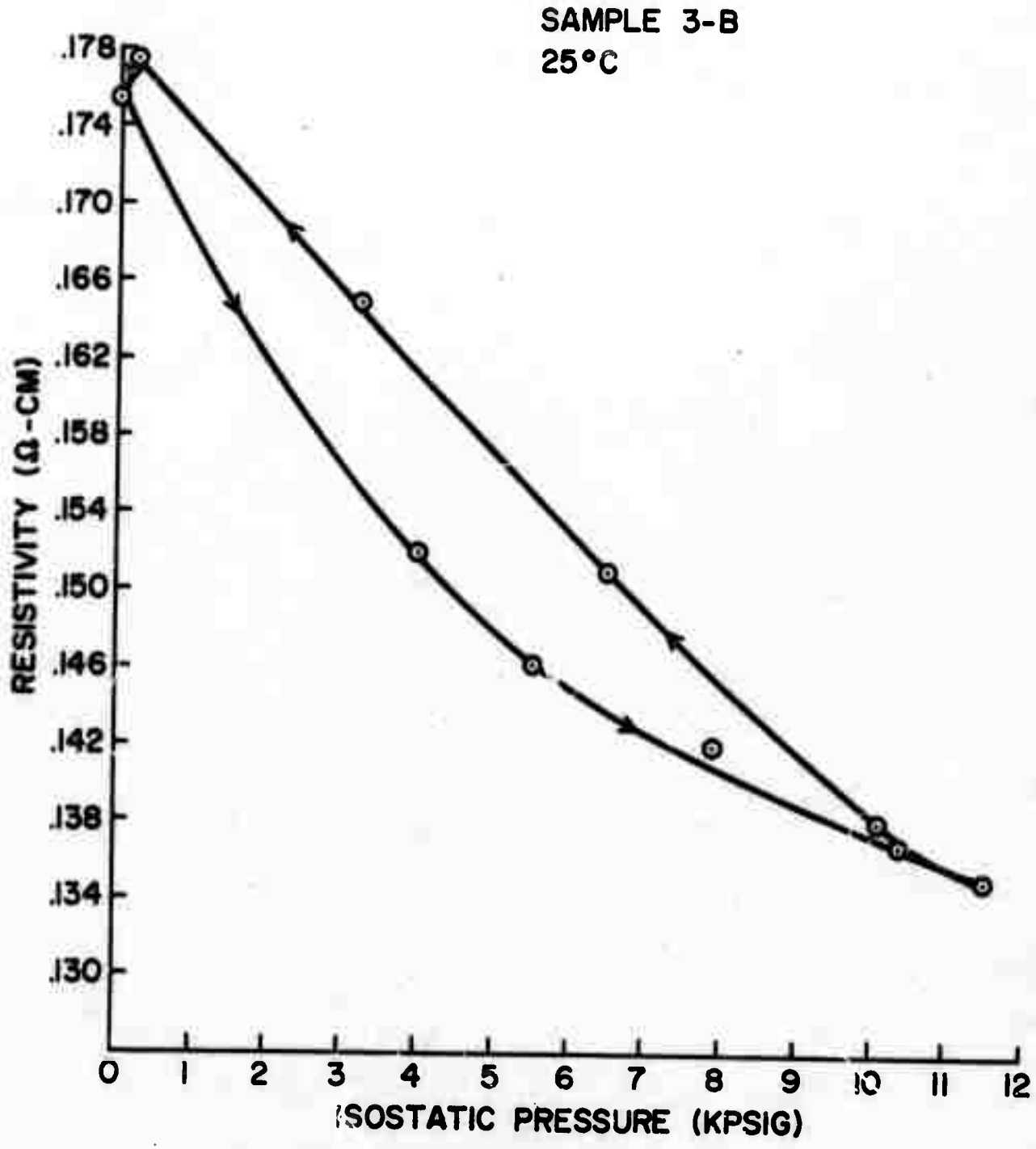

Figure 9. Resistivity versus Isostatic Pressure of a Compacted Sample of RuO_2 Powder

Run No.	T(°C)	$R_o/R_{12,000}$
4	101	1.08
5	64	1.09
6	35	1.09
7	36	1.06
8	104	1.08
9	115	1.09
10	125	1.06
12	50	1.02

The pressure coefficient of contact resistance is small and essentially temperature independent. Accurate values for the temperature coefficient of contact resistance at constant pressure could not be obtained because the changes in contact resistance resulting from pressure cycling were greater than the changes due to temperature. However, it can be concluded that the temperature coefficient of contact resistance is near zero and in no case can it be greater than $\pm$ 300 ppm/°C.

Based on all of our results the only way in which contact resistance between RuO_2 grains could be involved in the charge transport mechanism would be if the entire measured resistance of a thick film resistor is due to contact resistance. This possibility becomes unlikely when one considers the low noise characteristics of thick film resistors.

B. Formulation Rheology

1. Definition of Terms

The viscosity of a fluid is related to its flow (rate of shear) versus applied stress. Figure 10 shows several typical relationships between these two variables. Curve A of Figure 10 represents a Newtonian liquid for which the rate of shear is proportional to the shearing

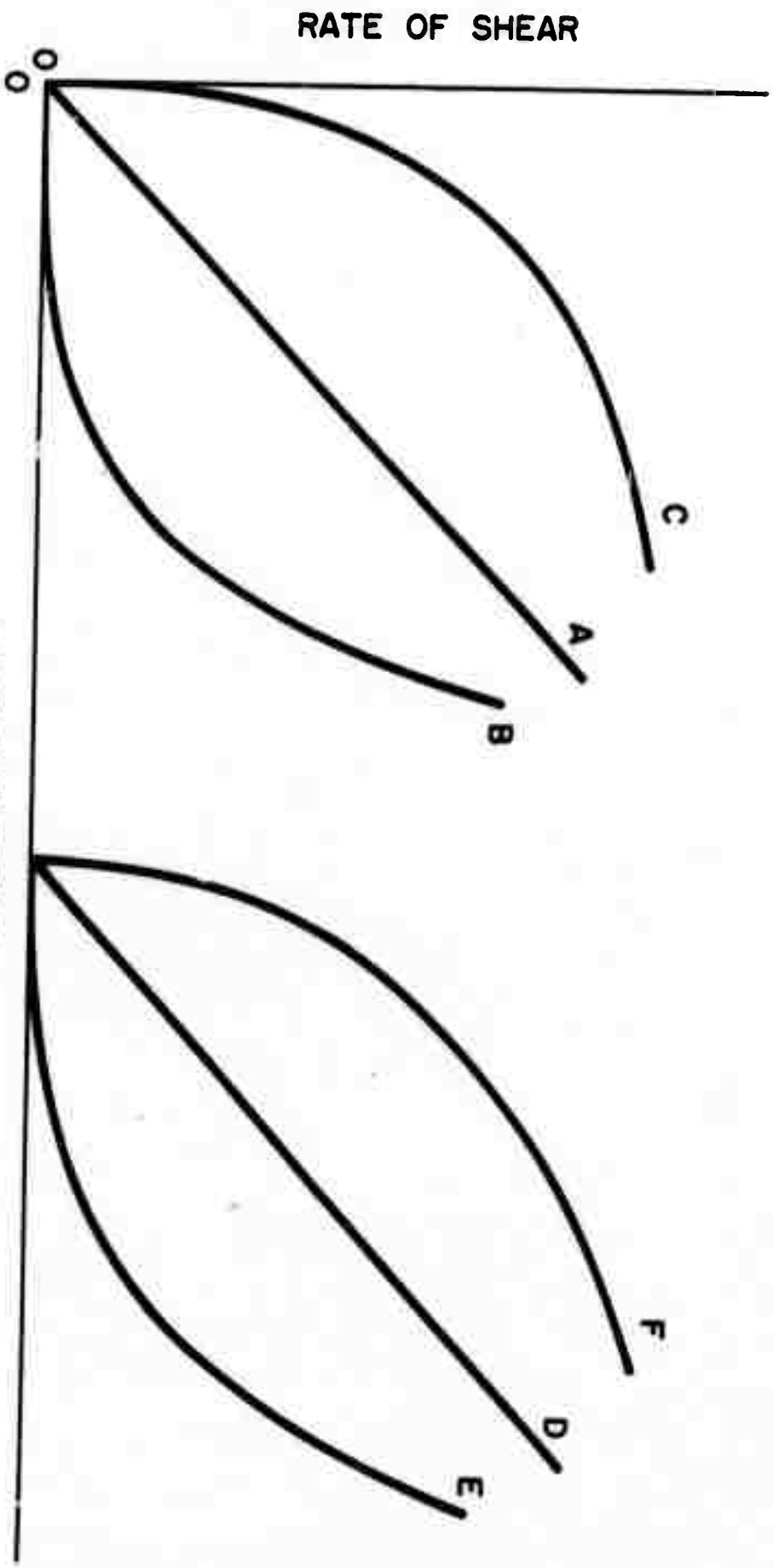

Figure 10. Generalized Rheological Behavior

stress. In the cgs system the units of shear stress are dynes/cm^2, the units of shear rate are sec^{-1} and the viscosity, or more correctly the coefficient of viscosity, is equal to the stress/rate of shear and has the units of poise (dyne-sec/cm^2) although centipoise is frequently used. The other five curves deviate from this simple relationship. Curve B represents a pseudoplastic fluid, C represents a dilatent fluid and D, E, and F represent fluids that have a yield value. A fluid with the stress versus shear rate dependence of Curve D is a Bingham plastic and curves E and F are pseudo-plastic and dilatant, respectively, with a yield value. None of these non-Newtonian fluids can be represented by a single, constant value of viscosity so two other parameters are used, both functions of the stress and shear rate. The apparent viscosity is equal to the applied stress divided by the corresponding rate of shear and the differential viscosity is equal to the slope of the curve. For non-Newtonian fluids the term viscosity usually implies apparent viscosity. Whether a fluid is Newtonian, pseudoplastic or dilatant can also be determined from a plot of log apparent viscosity versus log shear rate. Positive slopes are dilatant and negative slopes are pseudoplastic. Such graphs are usually close to straight lines which would indicated a power law relationship.

It should be mentioned that thixotropy is frequently confused with pseudoplasticity. A thixotropic fluid is one for which the viscosity at constant shear rate decreases with time, then increases again when the shear stress is removed. The times required for viscosity changes can vary from a fraction of a second to several hours. Of course, in the former case it is almost impossible to measure. The opposite of thixotropic is rheopectic.

2. Formulation Development and Characterization

The rheological properties of the complete formulation, screening agent plus inorganic powder, influences the screen printing operation, and there are two, somewhat separate steps to this operation. One is the transfer of fluid through the screen; this creates a non-uniform film consisting of cylinders separated by depressions caused by the screen wires. The second step is the leveling of the surface, hopefully without bleeding that would increase the area of the pattern. The viscosity requirements for these two steps are not necessarily the same.

Trease and Dietz [19] have estimated that the shear rate during screen printing is about 1000 sec^{-1}, and that the shear rate during leveling is about 0.1-0.01 sec^{-1}. They then evaluated the printing quality of several commercial formulations and compared the results with viscosity measurements at 100 sec^{-1} and 0.1 sec^{-1}, a convenient range for their instrument. They found that good transfer of material to the substrate required viscosities less than 500 poise at 100 sec^{-1} and that good leveling without bleedout required viscosities greater than 30,000 poise at 0.1 sec^{-1}. This approach is oversimplified; for example, leveling and viscosity are only partially related to one another since leveling is a surface phenomena and viscosity is a bulk property. That is, leveling can be changed with surface active (leveling) agents that do not appreciably affect viscosity. Nevertheless, their conclusions furnish a useful starting point in formulation development.

Screening agents for use in thick-film formulations are commercially available; presumably, they have been blended for optimum performance in terms of bleed-out, leveling, etc. Unfortunately, these

materials are propietary and chemically complicated so that their effect on the screened films during drying and firing is not clear. To minimize this type of uncertainty a screening agent was developed that is chemically simple though not optimum in other respects. Ethyl cellulose was chosen as the resin because its use in thick film formulations has been reported frequently in the past. The name ethyl cellulose does not represent an exact chemical formula, rather a family of materials that differ in the percent ethoxyl content. The substitution that takes place in the formation of the material is oxygen bonded ethyl groups in place of three hydroxyl groups per monomer unit. In general, the useful range of substitution is about 2.15 to 2.60 ethoxyl groups per unit or 43 to 50 w/o. The ethyl cellulose used in experimental formulations was obtained from Hercules and is classified as N-300, designating an ethoxyl content of 47.5-49 w/o, and implying that a 5% solution in 80:20 toluene; ethanol has a viscosity of 300 centipoise. Some work was also done with ethyl cellulose of lower ethoxyl content but it did not dissolve as well in the chosen solvent. No attempt was made to work with higher ethoxyl contents. The solvent chosen for use in the screening agent, diethylene glycol monobutyl ether (butyl carbitol) is not as commonly used but it has desirable vapor pressure versus temperature relationship, and seems to be adequate for use with the resin. A solution is formed by mixing the ethyl cellulose powder into heated butyl carbitol to accelerate the dissolution.

To characterize the screening agent a Brookfield Synchrolectric Model HET micro-viscometer was purchased along with the set of spindles that are commonly used in the thick-film industry. This permits a comparison of the prepared formulations with those that are commerically available. A Wells-Brookfield cone-plate viscometer attachment was

also obtained in order to measure viscosity or stress versus shear rate. The combination of cones and drive mechanisms permit the measurement of viscosity from 216 cps to 1.08×10^6 cps over the range 1 sec^{-1} to 750 sec^{-1} although, of course, the two parameters are interdependent.

Figure 11 shows the viscosity versus shear rate for three different concentrations of ethyl cellulose in butyl carbitol. The slopes of the lines indicate that the screening agents are slightly pseudoplastic, and a plot of shear rate versus stress shows that there is no observable yield value. An attempt was made to form a ten percent solution but there was some indication that not all of the ethyl cellulose dissolved.

Figure 12 shows the viscosity versus shear rate of a formulation consisting of a volume ratio of glass to screening agent of 40% using a screening agent that is 5% by weight ethyl cellulose. Based on earlier work [19] the formulation is not as pseudoplastic as is desirable but it has performed adequately in the experiments conducted up to the present. Initial tests indicate a small amount of thixotropy.

3. Substrate Cleaning and Drying

An important aspect of this project is the development of an ability to duplicate, on a laboratory scale, processes typical of industrial production including the areas of formulation preparation, screening, drying and firing. This is necessary because several of the planned experiments require screen printed samples that have been processed as uniformly as possible, and because it is important to test the ideas developed in the scientific phase under industrial conditions. A screening machine and a tunnel kiln have been installed, and initial results on cleaning the substrates and drying to constant weight are reported.

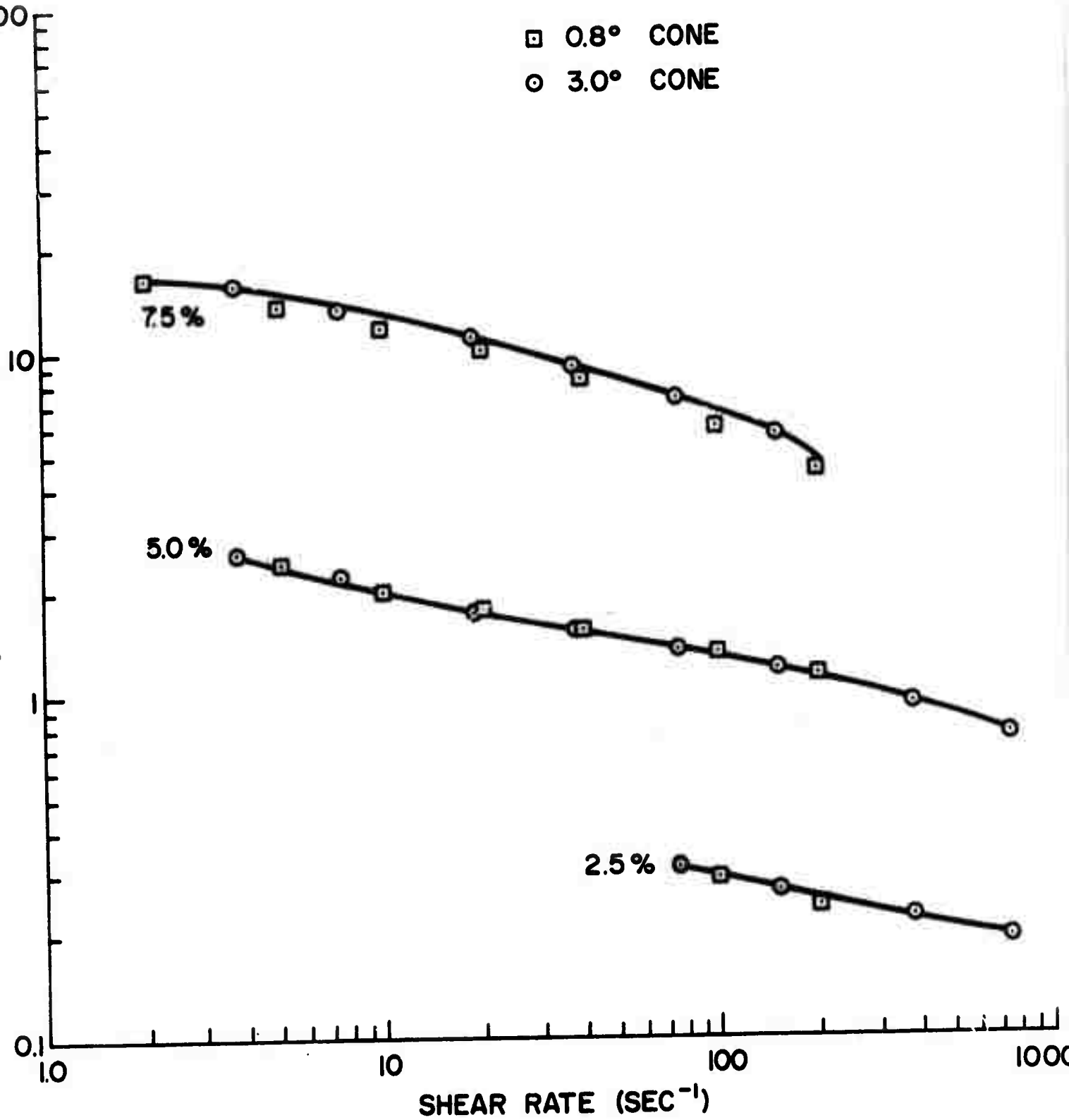

Figure 11. Rheological Behavior of Ethyl Cellulose-Butyl Carbitol Solutions

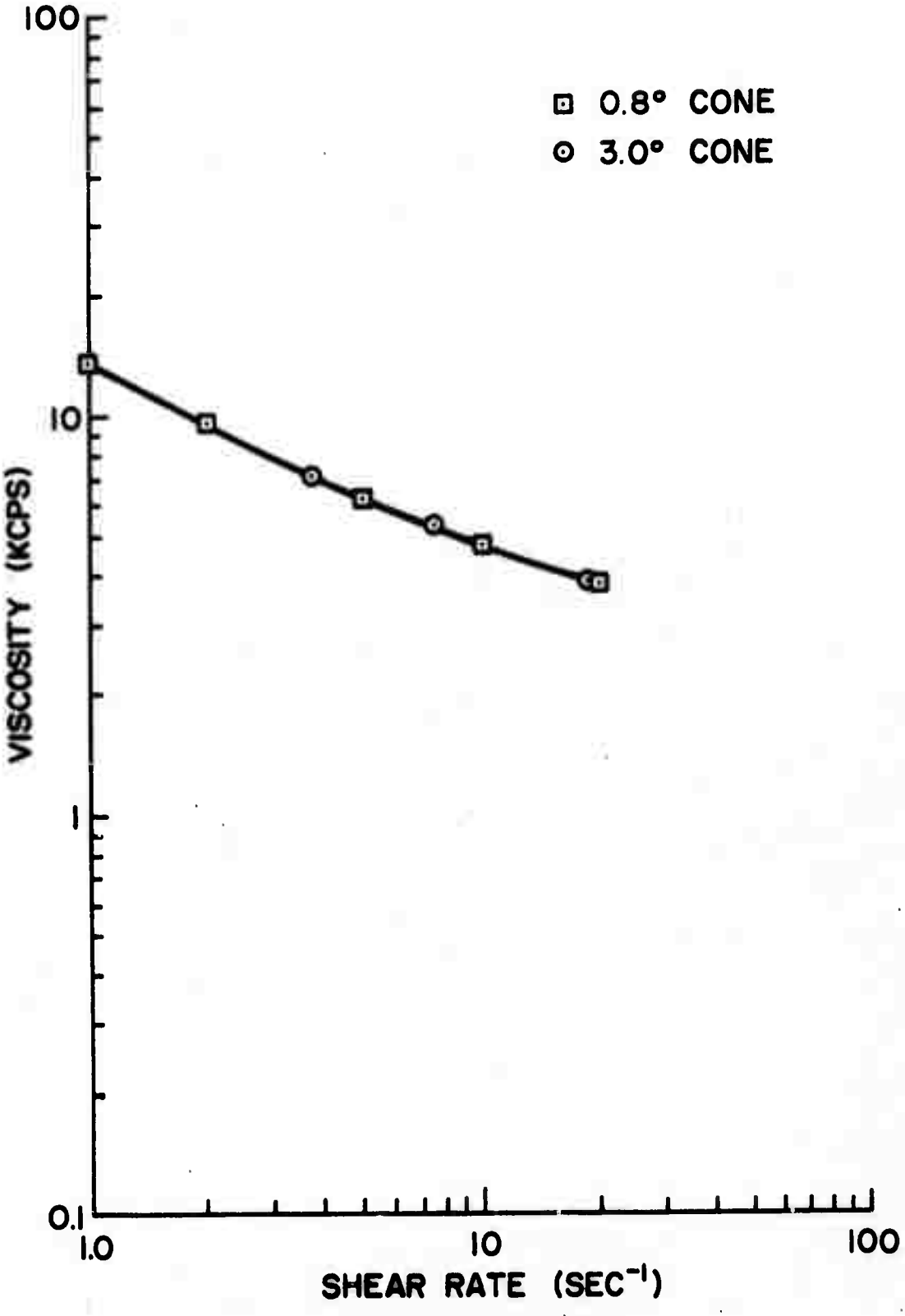

Figure 12. Rheological Behavior of a Formulation Containing 40 v/o Glass

The first step in evaluating the screen printer will be based on the weight of material deposited. To minimize weight changes of the substrate and in preparation of future work requiring clean substrates, procedures have been developed for cleaning the substrates and firing to constant weight (within the ability to weigh, about $\pm$ 0.3 milligrams). Two basic methods of cleaning were tested; one using hot acid baths and the other using a detergent, in both cases followed by rinsing and drying. A comparison, based on visual observations, subsequent weighing and firing steps, and discussions with industrial personnel evolved with cleaning alumina substrates for thin film circuits indicated that the proper use of a good detergent is adequate and less troublesome than the use of acids. The procedure is to ultrasonically clean with a warm detergent solution, rinse repeatedly in increasing purities of water, rinse in reagent grade methanol or isopropyl alcohol and dry for twenty minutes at 250°C. Fortunately, the cleaning requirements of the substrates are lessened by the nature of their manufacture. The high temperature firing required to form the substrates either volitilizes any contaminants or allows them to diffuse into the surface where they can no longer be removed by cleaning and they are usually handled carefully thereafter (nylon gloves, etc.). In fact, the method of cleaning recommended by one substrate supplier is to fire at a temperature greater than 900°C for at least 30 minutes. However, when preceeded by adequate chemical cleaning and drying at 250°C, no further weight or visual appearance changes were observed if the substrates were subsequently fired to a high temperature. Some of the initial cleaning attempts resulted a small amount of brown-yellow film on some substrates. The high temperature firing seemed to be adequate for removing this.

To eliminate a potential source of variation in weight, the substrates are kept in a desicated container as often as is reasonable, both after cleaning and drying and after screening and drying. The balance also contains desicant and carrier racks have been built to minimize transfer time.

IV. Summary and Future Plans

A self consistant model for the formation of resistor microstructure has been developed. The model is successful in that it correlates observed effects, but its predictive capability is yet to be established. A virtue of the model is that the individual steps required are amenable to experimental varification. If the model stands the test of experiment it will lead directly to the development of relationships between basic material properties and electrical characteristics of thick film resistors. This would produce somewhat of a deviation from current practice; material properties such as interfacial energies, diffusion coefficients, viscosities, and particle size distributions are not commonly considered in selecting thick film materials.

Various sources of potential error in resistor values have been considered. Theoretical expressions have been developed to account for various non-uniform resistor geometries. The characterization of formulation rheology has been initiated.

Completion of the studies of contact resistance between RuO_2 particles has resulted in the conclusion that the dominant conduction mechanism in thick film resistors is not intimately related to changes in the contact resistance between adjacent RuO_2 particles.

Studies to be continued or initiated during the coming period include:

1. Sintering Studies

The steps postulated for the microstructure model will be studied. Model experiments to measure the rate of neck growth between spherical particles of both glass and RuO_2 in the presence of glass will be conducted to determine the kinetics of the various sintering processes. These measurements will be made by hot stage microscopy with spheres in the 10μm range in order to slow the kinetics to a measurable rate. The important material parameters are surface tension and viscosity of the glass, conductive-glass interfacial energy, and solubility and diffusivity of the conductive in the glass.

2. Conductive Alloy Formation

Noble alloys for conductives are often assumed to be formed during firing of a formulation containing find powders of the pure metals. The degree of alloy formation is particularly important for alloys containing gold, silver, or palladium; pure gold and silver exhibit excessive solder leaching, and pure palladium exhibits excessive oxidation while proper alloys of these metals show a considerable reduction of these detrimental effects. High temperature x-ray diffraction techniques will be utilized to study the kinetics of alloy formation as a function of particle size. These results will then be compared with the kinetics of the sintering processes.

3. Particle Size Effects on the Resistivity of RuO_2

Previous studies on this project indicate that the apparent electrical properties of small particle size (50-100Å) RuO_2 may differ from that of the bulk, single crystal values; the electrical

resistivity may be greater by a factor of about three and the TCR lower by about the same factor. A possible explanation for these phenomina is that the scattering of the conduction electrons is increased due to increased crystal defects. The procedure for determining the resistivity of the powder will be to uniformly disperse the powder in a proper matrix, measure the resistivity of the composite, and apply the proper mixing rules. A review of hetrogeneous microstructures and the associated mixing rules shows that for maximum sensitivity to the resistivity of the dispersed phase (RuO_2), the resistivity of the matrix material should not be greater than ten times the resistivity of the powder. A microstructural analysis of the cooled composite will be made to determine the degree of dispersion and grain size of the matrix. Knowledge of these parameters is necessary for proper application of the mixing rules.

Previous measurements with single crystal RuO_2 down to 2μm diameter have failed to show any size effects; the TCR was identical to that of more massive single crystals. Thus, size effects can only be important below this size. Using powder at least as large as 1μm in diameter, as is planned, will allow verification of the measurement technique.

4. Electrical Properties of the RuO_2 Interface Region

Even though results reported previously indicate that the electrical properties of small particle size RuO_2 are significantly different from those of massive single crystal RuO_2, the differences are not great enough to explain the nearly-zero and sometimes negative TCR observed with thick film RuO_2 resistors. This phenomenon must be due to an additional effect resulting from the sintering process. An attempt will be made to better characterize the "contact" resistance between adjacent

regions of RuO_2 in the glass by continuing the experiments with the crossed single crystals with glass at the interface and comparing the results with the RuO_2-glass composites discussed later. In some cases, the crystals will be precoated with glass before being placed in contact to insure glass in the interface. If the results of this work suggest that quantum mechanical tunneling is likely then experiments involving, for example, glass coated single crystals in mercury, will be performed in order to correctly model this conduction mechanism.

5. Microstructure of Resistors and Conductors

The details of microstructure associated with "good" resistors and conductors will be determined. Of prime importance is the identification of the conducting phases, their shape, size, distribution, composition, and interaction.

6. Glass-RuO_2 Composites

Research reported in this report established the variation with pressure of the contact resistance of RuO_2. Proposed research with RuO_2-glass composites will determine pressure effects in a resistor-like environment. Eight glasses in the PbO-B_2O_3-SiO_2 system with coefficients of linear thermal expansion varying from 5 to 10 x $10^{-6}/^{o}C$ will be used for fabricating the composites. The pressure on the particle contacts can be calculated from a knowledge of the relative thermal expansions and the softening points of the glasses after correcting for the pressure due to interface forces.

7. Effects of Substrate Expansion

Substrates with coefficients of linear thermal expansion varying from 2 to 10 x $10^{-6}/^{o}C$ have been obtained and flame sprayed with a thin

coating of alumina so that the resistor-substrate interface will be the same in all cases. The resistance and TCR of resistors printed and fired on these substrates will be measured and the results analyzed in light of the results obtained with the RuO_2-glass composites.

8. Test of Models

The sheet resistance and TCR of resistors and conductors will be determined as a function of volume fraction of conductive phase to glass, and as a function of particle size of the conducting phase and of the glass. The important glass parameters (viscosity and surface tension) will be varied at constant thermal expansion, and the results compared with predictions of the microstructure model and the interface model. Chemical additives which will alter the electrical properties according to the interface model, but which will not effect microstructure development will be utilized to further test the interfact model.

V. References

1. R.W. Vest, Semi-annual Technical Report for the Period 7/1/70 - 12/31/70, Purdue Research Foundation Grant No. DAHC 15-70-G7, ARPA Order No. 1642, February 1, 1971.

2. R.L. Coble and J.E. Burke in "Progress in Ceramic Science", J.E. Burke, Ed., Vol. III, p. 197, Pergamon Press, London (1963).

3. F. Thummler and W. Thomma, Met. Revs., No. 115, 69 (1967).

4. V.N. Eremenko, Yu. V. Naiolich, and I.A. Lavrinenko, "Liquid Phase Sintering", Consultants Bureau, New York (1970).

5. G.C. Kuczynski, "Physics and Chemistry of Sintering", to be published.

6. J. Frenkel, J. Phys. (USSR), 9, 385 (1945).

7. G.C. Kuczynski, B. Neuville, and H.P. Toner, J. Appl. Polymer Sci., 14, 2069 (1970).

8. G.C. Kuczynski, J. Appl. Phys., 20, 1160 (1949).

9. J.K. Mackenzi and R. Shuttleworth, Proc. Phys. Soc. (London), B62, 833 (1949).

10. G.C. Kuczynski, Trans. A.I.M.E., 185, 796 (1949).

11. W.D. Kingery and M. Berg, J. Appl. Phys., 26, 1205 (1955).

12. G.H.S. Price, C.J. Smithells, and S.V. Williams, J. Inst. Metals, 62, 239 (1938).

13. J.B. Cutler, J. Amer. Ceram. Soc., 52, 14 (1969).

14. W.S. Young, S.T. Rosmussen, and I.B. Cutler in "Ultrafine Ceramics", J.J. Burke, N.L. Reed, and V. Weiss, eds., p. 185, Syracuse Univ. Press, Syracuse, NY (1970).

15. W.S. Young and I.B. Cutler, J. Amer. Ceram. Soc., 53, 659 (1970).

16. D.L. Johnson, Phys. Sintering, 1, B1 (1969).

17. D.A. Venkatu and D.L. Johnson, J. Amer. Ceram. Soc., 54, 641 (1971).

18. R.W. Berry, P.M. Hall, and M.T. Harris, "Thin Film Technology", p. 491, Van Nostrand Reinhold Co., New York (1968).

19. R.E. Trease and R.L. Dietz, Solid State Tech., 15, 39 (1972).